Journal of Fluids and Structures (2001) **15,** 691–715
doi:10.1006/jfls.2000.0372, available online at http://www.idealibrary.com on IDEAL®

NUMERICAL SIMULATION OF THE FLOW INDUCED BY A TRANSVERSELY OSCILLATING INCLINED ELLIPTIC CYLINDER

S. J. D. D'ALESSIO

Department of Applied Mathematics, University of Waterloo
Waterloo, Ontario, Canada N2L 3G1

AND

S. KOCABIYIK*

Department of Mathematics and Statistics, Memorial University of Newfoundland
St. John's, Newfoundland, Canada A1C 5S7

(Received 8 September 1999, and in final form 10 October 2000)

The unsteady flow past an inclined elliptic cylinder which starts translating and oscillating impulsively from rest in a viscous fluid is numerically investigated for large Reynolds number. The flow is incompressible and two-dimensional, and the oscillations are harmonic. These oscillations are allowed in a direction perpendicular to the uniform oncoming flow having a magnitude which is less than or equal to the constant translational velocity. The investigation is based on an implicit finite difference/spectral scheme for integrating the unsteady Navier–Stokes equations expressed in a stream function/vorticity formulation. Present calculations are performed at a sufficiently large oscillation amplitude to induce separation. The effect of the maximum oscillatory-to-translational velocity ratio and of the angle of inclination on the laminar asymmetric wake evolution has been studied for a Reynolds number $R = 10^3$. The object of this study is to examine the effect of increase of velocity ratio on the near-wake structure as well as the hydrodynamic forces acting on the cylinder. Vortex dynamics close behind the cylinder are affected by the changing acceleration of the cylinder. An interesting phenomenon has been observed in the flow patterns depending upon the velocity ratio and the angle of inclination. A switch over in the nature of the fluctuations of the drag coefficients has been also observed with the increase of angle of inclination.

1. INTRODUCTION

THIS PAPER EXAMINES in an initial way the transverse vibrations of an inclined elliptic cylinder in the presence of an oncoming uniform stream. Not only do these transverse oscillations have practical consequences relating to the design of engineering structures, but from a fundamental standpoint the forced transverse oscillations of elliptic cylinders form an important and relatively unexplored class of oscillatory flows. An extraordinary feature of previous work is the enormous effort that has been expended on understanding circular-cylinder flow, with its attendant complex interplay between boundary-layer development and near-wake dynamics. For flows induced by an elliptic cylinder performing translational oscillations perpendicular to its generators, references may be made only to the works of

*Corresponding author

0889–9746/01/070691 + 25 $35.00/0

Davidson & Riley (1972), Okajima *et al.* (1975), Taneda (1977) and Badr & Kocabiyik (1997). These studies were concerned with the case of purely translational oscillations of an elliptic cylinder placed in a fluid and translational oscillations were allowed only about an axis which coincides with either the major or minor axis of the ellipse except for Okajima *et al.* For large values of a suitably defined Reynolds number, such a flow induces a steady streaming in the fluid that is confined to a thin boundary-layer region at the cylinder surface. A collision of these steady-streaming boundary layers has been first predicted and visualized by Davidson & Riley (1972), resulting in jets of fluid erupting symmetrically from the elliptic cylinder surface along the axis of the vibration. The stability of a class of flows that exhibit steady streaming was considered by Hall (1984). In particular, he considered in detail the stability of the flow induced by the transverse oscillations of both circular and inclined elliptic cylinders in a quiescent viscous fluid. In the case of cylinders of elliptic cross-section, Hall found that for any given eccentricity the most unstable configuration is when the cylinder oscillates parallel to its minor axis. Badr & Kocabiyik (1997) carried out a numerical study to calculate the symmetric flow properties for a cylinder axis ratio of 0·6 when the Reynolds number ranges between 500 and 10^3. Their calculations were performed within the range of sufficiently large oscillation amplitude to induce separation. It is noted that flows generated by oscillating elliptic cylinders share some common characteristics with those of bluff bodies like circular cylinders. One of the most comprehensive studies on a cylinder oscillating normal to the incident flow is that of Williamson & Roshko (1988). They reported, within a range of amplitude, a vortex pattern in which a set of vortex pairs convect downstream but out to one side (the side depends on the history of the flow) and takes on the appearance of a jet rather than a wake.

To our knowledge, from an extensive literature survey, only one study has been done by Okajima *et al.* (1975) on the problem of the flow past an elliptic cylinder which is forced to oscillate transversely to the oncoming uniform flow when the cylinder is positioned asymmetrically relative to the main flow. The same problem is considered in the present study. In the work of Okajima *et al.* the viscous flow around both stationary and transversely oscillating elliptic cylinders were calculated at $R = 40$ and 80 by means of a numerical solution of the Navier–Stokes equations. The application of their numerical calculation is limited to low Reynolds numbers and some experiments have been carried out to study the viscous flow around an oscillating elliptic cylinder to provide information over a wide range of Reynolds numbers: $40 \leq R \leq 2 \times 10^3$.

In the present work, we consider the two-dimensional flow caused by an infinitely long elliptic cylinder set in motion impulsively which translates with uniform velocity U and also undergoes a harmonic translational oscillation in the transverse direction to that of translation. The cylinder is assumed to be inclined to the horizontal direction at an angle η. The ellipse has major and minor axis of lengths $2a$ and $2b$, respectively, and the cylinder oscillates with the velocity $U_m \cos \omega t$, where $\omega = 2\pi f$ and f is the forced frequency of oscillation. The Reynolds number is defined by $R = 2aU/\nu$ where a and ν stand for the semi-major axis length of the ellipse and the kinematic viscosity, respectively. The velocity ratio $\alpha = U_m/U$, the forcing Strouhal number $\boldsymbol{\Omega} = a\omega/U$, angle of inclination η and the minor-to-major axis ratio of the ellipse $r = b/a$ serve as scaled control parameters. The goal of the study is to investigate the effects of the maximum oscillatory-to-translational velocity ratio and the angle of inclination on the flow structure in the near-wake region as well as on the hydrodynamic forces acting on the cylinder for a fixed Reynolds number of $R = 10^3$ and forcing Strouhal number of $\boldsymbol{\Omega} = \pi$. Numerical calculations are performed for moderate values of time for the combinations: $\eta = \pi/4$ and $\alpha = 0{\cdot}5$, 1·0 and for $\alpha = 0{\cdot}5$ with $\eta = \pi/4,\ \pi/2$. The minor-to-major axis ratio of elliptic cylinder for these cases is taken to be 0·5. Noticeable changes in the near-wake and in the forces take place as α and η increase and are reported.

The underlying assumption made in our study is that the flow remains two-dimensional and laminar. One can argue that for the large Reynolds number regime considered three-dimensional effects and turbulence may significantly alter the flow. In fact, experimental work conducted by Williamson (1988) for the case of a circular cylinder suggests that a three-dimensional transition occurs for $R > 178$. Szepessy & Bearman (1992) measured a fluctuating lift on a thin section of a large aspect-ratio fixed-circular cylinder and found that two-dimensional simulation schemes generally overestimate the root-mean-square value of the fluctuating lift. This observation has been substantiated by Graham (1993), who gathered numerical predictions for circular cylinder flow and compared them with experimental results. He found that above a Reynolds number of 150 the mean and fluctuating forces were generally overpredicted, with largest differences occurring in the fluctuating lift. It should also be noted that measured time histories of the fluctuating lift show a pronounced amplitude modulation whereas simulated time histories mostly display a constant amplitude, once the flow has settled. Although physically the wake may be three-dimensional, we believe that it can be represented reasonably well by a two-dimensional model in the near-wake region which this study focuses on. On the evidence that spanwise correlations of forces, wake velocities, etc. all increase with transverse cylinder vibration at a frequency at or near the vortex shedding [e.g., Toebes (1969), Ramberg & Griffin (1976), Novak & Tanaka (1977), Blackburn & Henderson (1999)] it is reasonable to suggest that harmonic motion of a long cylinder seems to suppress the three-dimensionality and produce flows that are more two-dimensional than their fixed-cylinder counterparts, at least in the near-wake region.

The investigation is based on the solution of Navier–Stokes equations in their vorticity/stream function formulation via a finite-difference method similar to that used by Staniforth (1972) and D'Alessio *et al.* (1999). These studies use a Fourier spectral method together with an implicit Crank–Nicolson time-marching procedure. The problem of unsteady uniform flow over a stationary inclined cylinder was investigated by Staniforth (1972) and the validity of his solution is limited to high Reynolds numbers and small times. D'Alessio *et al.*, on the other hand, considered a uniform flow past a thin inclined elliptic cylinder under rotary oscillation, their method is also applicable to cross-flow and in-line oscillations. In their work, the numerical technique of Staniforth (1972) was utilized successfully in computing the early development of the flow for moderate to high Reynolds numbers. It is noted that the flow structures in these cases are different from the present case and that the following features in the wake as well as in the force coefficients occur in the present case: (i) the production of double or triple co-rotating vortex pairs in the near wake, and (ii) a switch-over in the nature of the fluctuations of the drag coefficient.

2. GOVERNING EQUATIONS AND METHOD OF SOLUTION

We are concerned with the two-dimensional flow generated by an infinitely long elliptic cylinder whose axis coincides with the z-axis placed in a viscous incompressible fluid. The cylinder is inclined at an angle η to the x-axis and the major and minor axes are along the axes of x and y, respectively. The free stream, far from the cylinder surface, exhibits uniform velocity U in the horizontal direction. Initially, the cylinder is at rest and at time $t = 0$ it suddenly starts to oscillate in transverse direction to that of the uniform flow with velocity $V(t) = U_m \cos \omega t$ as shown in Figure 1.

A suitable frame of reference which translates and oscillates with the cylinder is employed. In this frame the unsteady dimensionless equations for a viscous incompressible

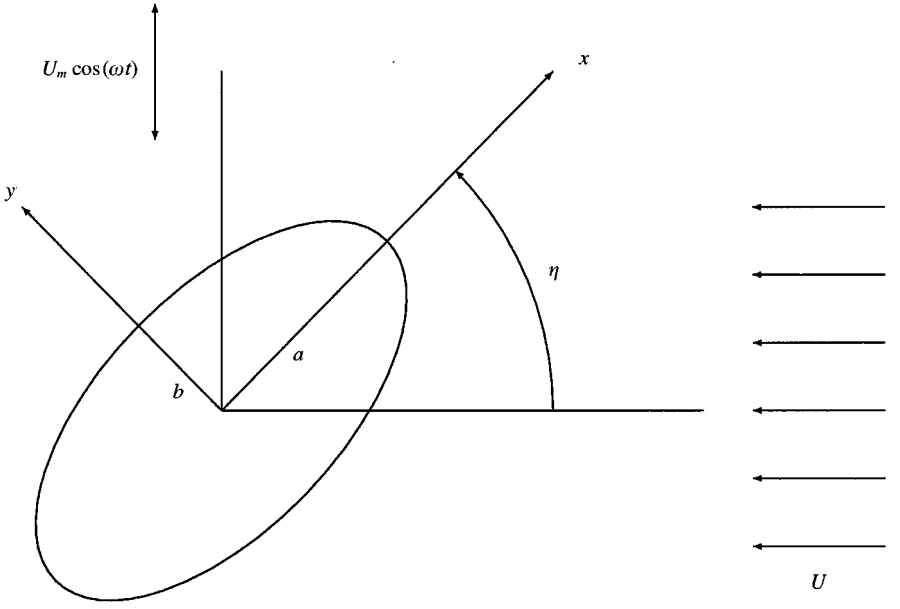

Figure 1. Coordinate system and flow configuration.

fluid in primitive variables can be written in vector form as

$$\frac{\partial \mathbf{v}}{\partial \tau} - \mathbf{v} \times \mathbf{w} = -\nabla\left(p + \frac{1}{2}|\mathbf{v}|^2\right) - \frac{2}{R}\nabla \times \mathbf{w} + \mathbf{a}, \tag{1}$$

$$\nabla \cdot \mathbf{v} = 0. \tag{2}$$

Here τ is the nondimensional time defined by $\tau = Ut/a$ and for the two-dimensional flow taking place in the xy-plane, the velocity $\mathbf{v} = (u, v, 0)$ and the vorticity $\boldsymbol{\omega} = \nabla \times \mathbf{v} = (0, 0, \zeta)$. The term $\mathbf{a}$ is the translational acceleration arising from the noninertial reference frame of the vibrating cylinder; specifically this acceleration is given by $-\dot{V}(\tau)(\sin\eta, \cos\eta, 0)$ where $V(\tau) = \alpha \cos \Omega\tau$ is the nondimensional oscillatory velocity of the cylinder and the dot denotes differentiation with respect to time τ.

Mathematically, an initial/boundary-value problem for two-dimensional Navier–Stokes equations must be solved. This solution is carried out in an elliptic coordinate (ξ, θ) system defined by the transformation

$$x + \mathrm{i}y = \cosh[(\xi + \xi_0) + \mathrm{i}\theta], \tag{3}$$

with the origin at the centre of the cylinder. Here the constant ξ_0 is defined by $\xi_0 = \tanh^{-1}(b/a)$ and $\xi = 0$ defines the surface of the cylinder. The governing equations in the elliptic coordinate system are

$$\frac{\partial^2 \psi}{\partial \xi^2} + \frac{\partial^2 \psi}{\partial \theta^2} = M^2 \zeta, \tag{4}$$

$$\frac{\partial \zeta}{\partial \tau} = \frac{1}{M^2}\left[\frac{2}{R}\left(\frac{\partial^2 \zeta}{\partial \xi^2} + \frac{\partial^2 \zeta}{\partial \theta^2}\right) + \left(\frac{\partial \psi}{\partial \theta}\frac{\partial \zeta}{\partial \xi} - \frac{\partial \psi}{\partial \xi}\frac{\partial \zeta}{\partial \theta}\right)\right]. \tag{5}$$

The dependent variables ψ and ζ in these equations are the dimensionless stream function and scalar vorticity, respectively, which are defined in terms of the usual dimensional stream

function ψ^* and vorticity ζ^* by $\psi^* = Ua\psi$ and $\zeta^* = U\zeta/a$ and M refers to the metric of the transformation (3) given by

$$M^2 = \frac{1}{2}[\cosh 2(\xi + \xi_0) - \cos 2\theta]. \tag{6}$$

The dimensionless velocity components (v_ξ, v_θ) in the directions of increase of (ξ,θ) are given by

$$v_\xi = -\frac{1}{M}\frac{\partial \psi}{\partial \theta}, \quad v_\theta = \frac{1}{M}\frac{\partial \psi}{\partial \xi}, \tag{7}$$

and the vorticity ζ is defined by

$$\zeta = \frac{1}{M^2}\left[-\frac{\partial}{\partial \theta}(Mv_\xi) + \frac{\partial}{\partial \xi}(Mv_\theta)\right]. \tag{8}$$

It is noted that if $\mathbf{u}$ and $\mathbf{v}$ denote the nondimensional velocities in the fixed and noninertial frames, respectively, then we have that

$$\mathbf{u} = \mathbf{v} + (\alpha \sin\eta \cos(\Omega\tau), \quad \alpha \cos\eta \cos(\Omega\tau))$$

and leads to equation (1). Thus, the stream function in the fixed frame $\bar{\psi}$ is related to the stream function in the noninertial frame ψ through

$$\bar{\psi} = \psi + \alpha \cos\eta \cos(\Omega\tau)x - \alpha \sin\eta \cos(\Omega\tau)\, y + C(\tau),$$

where $C(\tau)$ refers to an arbitrary function of time. The vorticities in the two frames, on the other hand, can easily be shown to be the same (i.e., $\bar{\zeta} = \zeta$). Using these along with the conformal transformation given by equation (3) one can obtain the equations given by equations (4) and (5). The conformal transformation applied is standard and has been used in several studies [see for example D'Alessio *et al.* (1999)]. The boundary conditions for $\tau > 0$ and $0 \le \theta \le 2\pi$ are the no-slip and impermeability conditions at the solid surface, and the free-stream conditions far away from it are given by

$$\psi = \frac{\partial \psi}{\partial \xi} = 0 \quad \text{when } \xi = 0, \tag{9}$$

$$\frac{\partial \psi}{\partial \xi} \to \frac{1}{2}\mathrm{e}^{\xi + \xi_0}[\sin(\theta + \eta) - \alpha \cos(\Omega\tau)\cos(\theta + \eta)] \quad \text{as } \xi \to \infty, \tag{10a}$$

$$\frac{\partial \psi}{\partial \theta} \to \frac{1}{2}\mathrm{e}^{\xi + \xi_0}[\cos(\theta + \eta) + \alpha \cos(\Omega\tau)\sin(\theta + \eta)] \quad \text{as } \xi \to \infty. \tag{10b}$$

Here the cylinder oscillation enters through the parameter $\Omega = a\,\omega/U$. The conditions in equation (10) lead to

$$\psi \to \tfrac{1}{2}\mathrm{e}^{\xi + \xi_0}[\sin(\theta + \eta) - \alpha \cos(\Omega\tau)\cos(\theta + \eta)] \quad \text{as } \xi \to \infty. \tag{11}$$

As a consequence of condition (10) we must also have that

$$\zeta \to 0 \quad \text{as} \quad \xi \to \infty. \tag{12}$$

It is well known that for moderate to high Reynolds number flows, the effective viscous-dominated regions are basically restricted near and downstream of the body of the cylinder. Shed vortices weaken very slowly as they travel downstream, in fact they persist in the narrow wake with a thickness of $\mathcal{O}(R^{-1/2})$ for hundreds of characteristic lengths of the body, and then eventually the flow becomes irrotational.

All the dependent variables in the flow domain must be periodic functions of θ with period 2π. Thus, in particular, the periodicity conditions for ψ and ζ are

$$\psi(\xi, \theta + 2\pi, \tau) = \psi(\xi, \theta, \tau), \quad \zeta(\xi, \theta + 2\pi, \tau) = \zeta(\xi, \theta, \tau). \tag{13}$$

Detailed derivations of equations and boundary conditions similar to the ones used in this study were given in the works of Staniforth (1972) and D'Alessio *et al.* (1999) for the cases of unsteady uniform flow over a stationary inclined elliptic cylinder and a thin inclined elliptic cylinder under rotational oscillation, respectively. This section briefly summarizes the equations and the boundary conditions. It is noted that the far-field conditions given by equations (10a,b) differ from the ones given in these studies because of the differences between the reference frames as well as the cylinder motions. Also, the first condition of equation (9) is different from the one given by D'Alessio *et al.* due to the rotary oscillation of the ellipse in their work.

The boundary conditions for the stream function on the cylinder surface are overspecified and there is no explicit boundary condition for the vorticity on the cylinder surface. In principle, the surface vorticity can be computed from the known stream function by applying equation (4), however, the large velocity gradient at the surface reduces the accuracy of such computations. In this study, an integral condition is used to predict the surface vorticity. The overspecified local conditions can be utilized to obtain global vorticity conditions, termed integral conditions, and these conditions are derived by applying Green's identity for the Laplacian operator, namely

$$\iiint_V (\phi \nabla^2 \psi - \psi \nabla^2 \phi) \, \mathrm{d}V = \oint_S \left(\phi \frac{\partial \psi}{\partial n} - \psi \frac{\partial \psi}{\partial n} \right) \mathrm{d}s \tag{14}$$

to the flow domain V outside the cylinder following the work by Dennis & Quartapelle (1989) and Dennis & Kocabiyik (1991). Here boundary S of the flow domain is the contour of the cylinder itself together with a contour at a large distance from it and $\mathbf{n}$ refers to the outward normal to the boundary S of the flow domain and s is measured along it. Condition (14) is utilized by taking ϕ to be the harmonic functions $\phi = \{1, \mathrm{e}^{-n\xi} \cos n\theta, \mathrm{e}^{-n\xi} \sin n\theta : n = 1, 2, \ldots\}$ and using $\nabla^2 \psi = M^2 \zeta$ from equation (4), it is found, after use of equations (9) and (10) and some integration by parts, that

$$\int_0^\infty \int_0^{2\pi} M^2 \zeta(\xi, \theta, \tau) \, \mathrm{d}\theta \, d\xi = 0, \tag{15a}$$

$$\int_0^\infty \int_0^{2\pi} \mathrm{e}^{-n\xi} M^2 \zeta(\xi, \theta, \tau) \cos(n\theta) \, \mathrm{d}\theta \, \mathrm{d}\xi = \pi \mathrm{e}^{\xi_0} [\sin \eta - \alpha \cos(\Omega\tau) \cos \eta] \, \delta_{1,n}, \tag{15b}$$

$$\int_0^\infty \int_0^{2\pi} \mathrm{e}^{-n\xi} M^2 \zeta(\xi, \theta, \tau) \sin(n\theta) \, \mathrm{d}\theta \, \mathrm{d}\xi = \pi \mathrm{e}^{\xi_0} [\cos \eta + \alpha \cos(\Omega\tau) \sin \eta] \, \delta_{1,n} \tag{15c}$$

for all integers $n \geq 1$; $\delta_{m,n}$ is the Kronecker delta symbol defined by

$$\delta_{m,n} = 1 \text{ if } m = n, \quad \delta_{m,n} = 0 \text{ if } m \neq n.$$

Finally, an initial condition is necessary to start the flow. Boundary-layer theory for impulsively started flows is used to provide this by utilizing the boundary-layer transformation

$$\xi = kz, \quad \psi = k\Psi, \quad \zeta = \omega/k, \quad k = 2(2\tau/R)^{1/2}, \tag{16}$$

which maps the initial flow onto the scale of the boundary-layer thickness. This change of variables removes the singularity in the vorticity at $\tau = 0$ due to the impulsive start. We emphasize that although boundary-layer coordinates are utilized, the full Navier–Stokes

equations are to be solved and not the simplified boundary-layer equations. In terms of these boundary-layer coordinates the governing equations become

$$\frac{\partial^2 \Psi}{\partial z^2} + k^2 \frac{\partial^2 \Psi}{\partial \theta^2} = M_z^2 \omega, \tag{17}$$

$$\frac{1}{M_z^2}\frac{\partial^2 \omega}{\partial z^2} + 2z\frac{\partial \omega}{\partial z} + 2\omega = 4\tau\frac{\partial \omega}{\partial \tau} - \frac{k^2}{M_z^2}\frac{\partial^2 \omega}{\partial \theta^2} - \frac{4\tau}{M_z^2}\left(\frac{\partial \Psi}{\partial \theta}\frac{\partial \omega}{\partial z} - \frac{\partial \Psi}{\partial z}\frac{\partial \omega}{\partial \theta}\right), \tag{18}$$

where $M_z^2 = [\cosh 2(kz + \xi_0) - \cos 2\theta]$ and the solution of these equations are now required subject to the conditions

$$\Psi = \frac{\partial \Psi}{\partial z} = 0 \quad \text{when } z = 0, \tag{19}$$

$$\int_0^\infty \int_0^{2\pi} M_z^2\, \omega(z, \theta, \tau)\, \mathrm{d}\theta\, \mathrm{d}z = 0, \tag{20a}$$

$$\int_0^\infty \int_0^{2\pi} \mathrm{e}^{-nkz} M_z^2\, \omega(z, \theta, \tau) \cos(n\theta)\, \mathrm{d}\theta\, \mathrm{d}z = \pi \mathrm{e}^{\xi_0} [\sin\eta - \alpha \cos(\Omega\tau)\cos\eta]\, \delta_{1,n}, \tag{20b}$$

$$\int_0^\infty \int_0^{2\pi} \mathrm{e}^{-nkz} M_z^2\, \omega(\xi, \theta, \tau) \sin(n\theta)\, \mathrm{d}\theta\, \mathrm{d}z = \pi \mathrm{e}^{\xi_0} [\cos\eta + \alpha \cos(\Omega\tau)\sin\eta]\, \delta_{1,n} \tag{20c}$$

for all integers $n \geq 1$.The transformed Navier–Stokes equations (17) and (18) are solved subject to equations (19) and (20) entirely in terms of the new variables (16). This is possible if the Reynolds number is high enough, but for small R the boundary-layer thickness k soon grows and it is then more realistic to continue the integration in the physical coordinate ξ so that the grid size in the actual physical space does not become too large. The equations governing the initial solution can be determined by setting $\tau = 0$ and hence $k = 0$ for any value of R in equations (17) and (18). The equations for $\Psi_0 \equiv \Psi(z, \theta, 0)$ and $\omega_0 \equiv \omega(z, \omega, 0)$ are

$$\frac{\partial^2 \Psi_0}{\partial z^2} = M_0^2 \omega_0, \quad \frac{1}{M_0^2}\frac{\partial^2 \omega_0}{\partial z^2} + 2z\frac{\partial \omega_0}{\partial z} + 2\omega_0 = 0, \tag{21a,b}$$

where $M_0^2 = \frac{1}{2}[\cosh(2\xi_0) - \cos(2\theta)]$ is the value of M_z^2 on the cylinder surface $z = 0$. The solutions of these equations satisfying equations (19) and (20) are

$$\omega_0(z, \theta, 0) = \frac{2}{\sqrt{\pi}}\frac{\mathrm{e}^{\xi_0}}{M_0}[\sin(\theta + \eta) - \alpha\cos(\theta + \eta)]\, \mathrm{e}^{-M_0^2 z^2}, \tag{22a}$$

$$\Psi_0(z, \theta, 0) = \frac{\mathrm{e}^{\xi_0}}{M_0}[\sin(\theta + \eta) - \alpha\cos(\theta + \eta)]\left[M_0 z\, \mathrm{erf}(M_0 z) - \frac{1}{\sqrt{\pi}}(1 - \mathrm{e}^{-M_0^2 z^2})\right], \tag{22b}$$

where $\mathrm{erf}(M_0 z)$ denotes the error function. This initial solution forms the starting point of the numerical integration procedure.

3. COMPUTATIONAL METHOD OF SOLUTION

The Navier–Stokes equations (17) and (18) in terms of the variables (z, θ) are solved by finite differences using a Gauss–Seidel iterative procedure with under-relaxation applied only to the surface vorticity. The method is based on approximating the stream function using a Fourier series expansion and is essentially a generalization of the method used by

Staniforth (1972) that takes into consideration the effect of transverse cylinder oscillations; therefore, this section only briefly summarizes the equations and numerics. The computational domain bounded by $0 \leq z \leq z_\infty$ and $0 < \theta < 2\pi$, is discretized into a network of $L \times P$ grid points located at

$$z_i = ih, \quad i = 0, \quad 1, \ldots, L \quad \text{where } h = z_\infty / L, \tag{23}$$

$$\theta_i = i\lambda, \quad i = 0, \quad 1, \ldots, P \text{ where } \lambda = 2\pi / P. \tag{24}$$

Here z_∞ refers to the outer boundary approximating infinity. Placing z_∞ well outside the growing boundary layer enables us to enforce the free-stream condition (10) along the line $z = z_\infty$. Expressed in terms of the boundary-layer coordinates (z, θ) this condition becomes

$$\mathrm{e}^{-kz} \frac{\partial \Psi}{\partial z} \to \frac{1}{2} \mathrm{e}^{\xi_0} [\sin(\theta + \eta) - \alpha \cos(\Omega\tau) \cos(\theta + \eta)] \quad \text{as } z \to \infty, \tag{25a}$$

$$\mathrm{e}^{-kz} \frac{\partial \Psi}{\partial \theta} \to \frac{1}{2k} \mathrm{e}^{\xi_0} [\cos(\theta + \eta) + \alpha \cos(\Omega\tau) \sin(\theta + \eta)] \quad \text{as } z \to \infty. \tag{25b}$$

We point out that the physical coordinate $\xi = kz$ is a moving coordinate and hence the outer boundary $\xi_\infty = kz_\infty$ is constantly being pushed further away from the cylinder surface at a rate which reflects the growth of the boundary layer. For this reason we are justified in saying that the vorticity, by the mechanism of convection, does not reach the outer boundary ξ_∞. It is noted that the grid is not uniform in the x or y directions. The spacing is such that the grid points are spaced closer together near the surface and further apart at larger distances. In addition, the adopted grid mesh is continually growing in time to properly accommodate the vortex shedding process. Figure 2 illustrates how the grid expands for the case of $R = 10^3$ and $\eta = \pi/4$ for an ellipse having $r = 0{\cdot}5$ at times $\tau = 0{\cdot}1$ and 1. Shown are 10 equally spaced grid lines for $0 \leq z \leq z_\infty$. If z_∞ is chosen to be large enough then as time increases the outer boundary will expand and be far enough away that no shed vortices will have reached it. If this is so, then we can correctly apply the condition of zero vorticity along the outer boundary. Although shed vortices propagate faster than the

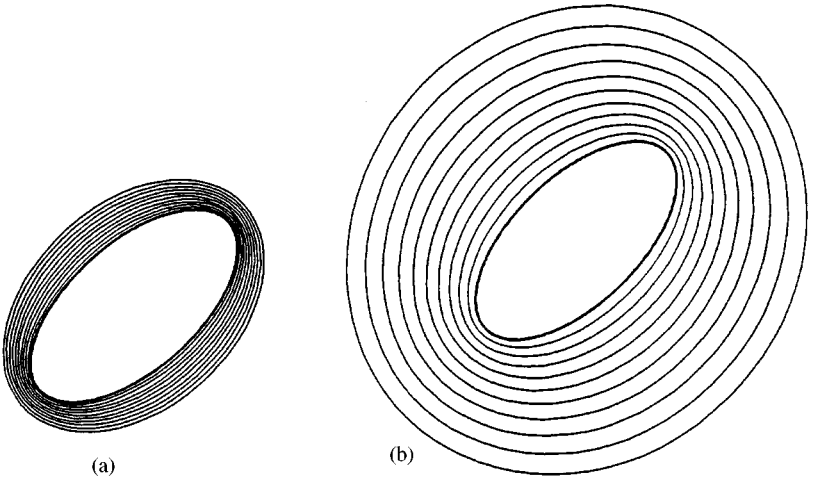

Figure 2. An illustration to show how the grid expands with time when $R = 10^3$ and $\eta = \pi/4$: (a) $\tau = 0{\cdot}1$, and (b) $1{\cdot}0$.

rate of boundary-layer growth, they weaken as they travel downstream in the wake. Clearly, as time increases we may encounter a problem whereby the vorticity reaches the boundary, but for the cases and times considered in our study this is not the case.

We solve for the stream function by expanding it into a Fourier series given by

$$\Psi(z,\theta,\tau) = \frac{1}{2} F_0(z,\tau) + \sum_{n=1}^{\infty} (F_n(z,\tau)\cos n\theta + f_n(z,\tau)\sin n\theta). \tag{26}$$

The equations governing the functions in equation (26) are

$$\frac{\partial^2 F_n}{\partial z^2} - n^2 k^2 F_n = s_n(z,\tau), \quad n = 0, 1, \ldots, \tag{27a}$$

$$\frac{\partial^2 f_n}{\partial z^2} - n^2 k^2 f_n = r_n(z,\tau), \quad n = 1, \ldots, \tag{27b}$$

where

$$s_n = \frac{1}{\pi}\int_0^{2\pi} M^2\,\omega(z,\theta,\tau)\cos n\theta\,\mathrm{d}\theta, \quad r_n = \frac{1}{\pi}\int_0^{2\pi} M^2\omega(z,\theta,\tau)\sin n\theta\,\mathrm{d}\theta. \tag{28a,b}$$

Boundary conditions for the Fourier components of Ψ are

$$F_0(0,\tau) = F_n(0,\tau) = f_n(0,\tau) = 0, \quad \frac{\partial F_0}{\partial z} = \frac{\partial F_n}{\partial z} = \frac{\partial f_n}{\partial z} = 0 \quad \text{when } z = 0, \tag{29}$$

and as $z \to \infty$

$$\mathrm{e}^{-kz} F_0 \to 0, \quad \mathrm{e}^{-kz}\frac{\partial F_0}{\partial z} \to 0, \tag{30a}$$

$$\mathrm{e}^{-kz} F_n \to \frac{1}{2k}\mathrm{e}^{\xi_0}[\sin\eta - \alpha\cos(\Omega\tau)\cos\eta]\,\delta_{n,1}, \quad \mathrm{e}^{-kz}\frac{\partial F_n}{\partial z} \to \frac{1}{2}\mathrm{e}^{\xi_0}[\sin\eta - \alpha\cos(\Omega\tau)\cos\eta]\,\delta_{n,1}, \tag{30b}$$

$$\mathrm{e}^{-kz} f_n \to \frac{1}{2k}\mathrm{e}^{\xi_0}[\cos\eta + \alpha\cos(\Omega\tau)\sin\eta]\,\delta_{n,1}, \quad \mathrm{e}^{-kz}\frac{\partial f_n}{\partial z} \to \frac{1}{2}\mathrm{e}^{\xi_0}[\cos\eta + \alpha\cos(\Omega\tau)\sin\eta]\,\delta_{n,1} \tag{30c}$$

for $n = 1, 2, \ldots$.

Further conditions satisfied by the functions $r_n(z,\tau)$ and $s_n(z,\tau)$ can be obtained by considering the properties of the solutions to equations (27a,b) together with their corresponding boundary conditions (29) and (30). These conditions are of a global or integral nature and are exact; they also play an important role in the determination of the surface vorticity and are given by

$$\int_0^{\infty} s_0(z,\tau)\,\mathrm{d}\theta\,\mathrm{d}z = 0, \tag{31a}$$

$$\int_0^{\infty} \mathrm{e}^{-nkz} s_n(z,\tau)\,\mathrm{d}z = \mathrm{e}^{\xi_0}[\sin\eta - \alpha\cos(\Omega\tau)\cos\eta]\,\delta_{1,n}, \tag{31b}$$

$$\int_0^{\infty} \mathrm{e}^{-nkz} r_n(z,t)\,\mathrm{d}z = \mathrm{e}^{\xi_0}[\cos\eta + \alpha\cos(\Omega\tau)\sin\eta]\,\delta_{1,n}. \tag{31c}$$

Equations (27a,b) at a fixed value of τ are of the form

$$h''(z) - \beta^2 h(z) = g(z), \tag{32}$$

where $\beta = nk$ and the prime refers to differentiation with respect to z. These ordinary differential equations can be integrated using step-by-step formulae. The important point to note here is that the particular marching algorithm to be used is dependent on the parameter β. Dennis & Chang (1969) have found that most step-by-step procedures become increasingly unstable as β becomes large. Hence, two sets of step-by-step methods were utilized: one for $\beta < 0{\cdot}5$ while another one for $\beta > 0{\cdot}5$. The specific schemes used will not be presented; however, these details can be found in Staniforth (1972). The vorticity transport equation (18) is solved by finite differences. Previous studies for the case of a circular cylinder have also expanded the vorticity in a Fourier series. In this instance, the metric given by $M^2 = e^{2\xi}$ is independent of θ. In our problem the metric, given by equation (6), depends on θ and consequently complicates matters if expressed in a Fourier series. Despite this, Patel (1981) and Badr (1994) for the case of inclined elliptic cases expanded the vorticity in a Fourier series and numerically solved the resulting partial differential equations for the Fourier coefficients. Badr (1994) carried out a very careful numerical study to deal with purely oscillating viscous flow past a stationary inclined elliptic cylinder. In his work, rectilinear flow oscillations are only allowed in the horizontal free-stream direction.

The scheme used to approximate equation (18) is very similar to the Crank–Nicolson implicit procedure. Equation (18) may be rewritten in the form

$$\tau \frac{\partial \omega}{\partial \tau} = q(z, \theta, \tau), \tag{33}$$

where

$$q(z, \theta, \tau) = \frac{1}{4M_z^2}\frac{\partial^2 \omega}{\partial z^2} + \frac{z}{2}\frac{\partial \omega}{\partial z} + \frac{\omega}{2} + \frac{k^2}{4M_z^2}\frac{\partial^2 \omega}{\partial \theta^2} + \frac{\tau}{M_z^2}\left(\frac{\partial \Psi}{\partial \theta}\frac{\partial \omega}{\partial z} - \frac{\partial \Psi}{\partial z}\frac{\partial \omega}{\partial \theta}\right). \tag{34}$$

It is the finite-difference approximation to the time derivative that enables us to advance the solution step-by-step in time. Assuming the solution at time τ is known, let us advance the solution to time $\tau + \Delta\tau$ by integrating equation (33). Integration by parts yields

$$\omega|_{\tau}^{\tau+\Delta\tau} - \int_{\tau}^{\tau+\Delta\tau} \omega \, d\tau = \int_{\tau}^{\tau+\Delta\tau} q \, d\tau, \tag{35}$$

where $\Delta\tau$ is the time increment. If we approximate the integrals using the trapezoidal rule this brings us to the expression

$$\omega(z, \theta, \tau + \Delta\tau) = \omega(z, \theta, \tau) + \frac{\Delta\tau}{2\tau + \Delta\tau}[q(z, \theta, \tau + \Delta\tau) + q(z, \theta, \tau)]. \tag{36}$$

Since $q(z, \theta, \tau + \Delta\tau)$ depends on $\omega(z, \theta, \tau + \Delta\tau)$ and its derivatives the scheme is implicit. Equation (36) is solved iteratively using the Gauss–Seidel procedure. All spatial derivatives appearing in equation (34) are approximated using central differences. The boundary conditions used in solving the vorticity transport equation include

$$\omega(z, \theta, \tau) = \omega(z, \theta + 2\pi, \tau) \tag{37}$$

and

$$\omega(z_\infty, \theta, \tau) = 0. \tag{38}$$

The surface vorticity is determined by inverting equations (28a,b); this leads to the following expression:

$$\omega(0,\theta,\tau)=\frac{1}{M_0^2}\left\{\frac{1}{2}s_0(0,\tau)+\sum_{n=1}^{\infty}\left[r_n(0,\tau)\sin n\theta+s_n(0,\tau)\cos n\theta\right]\right\}. \tag{38}$$

The integration procedure is initiated using the initial solution (22) at $\tau=0$. The use of this initial solution is essential for obtaining accurate results at small time. The use of a potential flow solution as an initial condition at $\tau=0$ has been frequently adopted by many researchers; however, this will definitely lead to inaccurate results following the start of the fluid motion.

We now summarize the numerical method by listing the numerical procedure. Assuming all quantities are known at time τ and wish to advance the solution to a time $\tau+\Delta\tau$, we perform the following steps (p denotes the iteration counter): (i) solve for $\omega^{(p)}(z,\theta,\tau+\Delta\tau)$ using equation (36) everywhere except on the cylinder surface ($z=0$); (ii) compute $r_n^{(p)}(z,\tau+\Delta\tau)$, $s_n^{(p)}(z,\tau+\Delta\tau)$ from equations (28a, b) for $z\neq 0$; (iii) calculate $r_n^{(p)}(0,\tau+\Delta\tau)$, $s_n^{(p)}(0,\tau+\Delta\tau)$ by enforcing the integral conditions (31a)–(31c) and hence compute $\omega^{(p)}(0,\theta,\tau+\Delta\tau)$ from equation (38); (iv) solve equations (27a,b) for $f_n^{(p)}(z,\tau+\Delta\tau)$, $F_n^{(p)}(z,\tau+\Delta\tau)$ and thus obtain $\Psi^{(p)}(z,\theta,\tau+\Delta\tau)$ using equation (26); and (v) repeat above steps till convergence is reached and increment p by 1 after each complete iteration.

Step (3) indicates how the integral conditions are used in determining the surface vorticity. It may also be necessary to subject the surface vorticity to under-relaxation in order to obtain convergence. Convergence is reached when the difference between two successive iterates of the surface vorticity, $|\omega^{(p+1)}(0,\theta,\tau+\Delta\tau)-\omega^{(p)}(0,\theta,\tau+\Delta\tau)|$, falls below some specified tolerance ε. Typically, $\varepsilon=10^{-5}$ was used. It is noted that the integrals appearing in equations (28a)–(28c) were evaluated by Filon integration in order to guarantee consistent accuracy for all n. This technique bears a close resemblance to Simpson's rule with the exception that only the unknown part of the integrand is approximated by a parabola over three successive grid points rather than the entire integrand.

In the present calculations the maximum number of terms used in series (26) is $N=25$. Checks are made for $R=10^3$ at several typical values of τ to ensure that N is large enough. This is done by increasing N and observing that the solution did not change appreciably. Due to the impulsive start, small time steps are needed to get past the singularity at $\tau=0$. Initially, $\Delta\tau=10^{-5}$ is used; as time increases the time step is gradually increased until reaching $\tau=0{\cdot}01$. The number of points in the z-direction is taken as 201 with a space step of $\Delta z=0{\cdot}06$. This makes $z_\infty=12$ which sets the outer boundary at a physical distance of about 40 major axis lengths away for $R=10^3$ and time $\tau=12$. Thus, the boundary is sufficiently far away so that the application of the boundary conditions (30a)–(30c) does not affect the solution in the viscous region near the cylinder surface. The values of grid sizes are to some extent chosen to be comparable with those used by D'Alessio *et al.* (1999), since these were found to be satisfactory and were checked carefully. Moreover, this scheme is tested against the results of Staniforth (1972) for the nonoscillating (i.e., purely translating) case using similar Reynolds numbers; tests indicate that solutions are quite accurate. Finally, we note that the numerical method described may be used to continue the solution for increasing τ in terms of the physical coordinate ξ when the boundary layer thickens. However, in the present paper, only the case of $R=10^3$ is presented, and it is possible to work in terms of the boundary-layer coordinate z over the entire range of τ considered.

4. RESULTS AND DISCUSSION

Before presenting the results we first perform some accuracy checks on our numerical scheme. To do this, computations were carried out for purely translating inclined elliptic

cylinder ($\Omega = 0$, $\alpha = 0$) using the grid $L \times P = 121 \times 121$ when $\eta = \pi/2$ with $R = 250$, $r = 0{\cdot}5878$. The parameter values chosen allow comparison with the numerical results of Patel (1981) in which the Reynolds number R_c is based on the focal distance of the ellipse and defined by $R_c = U(2c)/\nu$. It is noted that $R_c = 200$ corresponds closely to $R = 250$. The variations of the vorticity at $\tau = 1$ and 5 are presented only for $0 \leq \theta \leq 180^\circ$ due to the symmetry and compared with the numerical solution obtained by Patel (1981) in Figure 3. Patel's numerical solution uses a potential flow solution as an initial condition whereas the present analysis uses the initial condition (22) obtained from the exact solution of full Navier–Stokes equations at $\tau = 0$. The agreement is found to be good and improves for $\tau = 5$ as the solution becomes more or less independent of the initial solution with the increase in time. Moreover, our numerical procedure for the purely translating case ($\Omega = 0$, $\alpha = 0$) when $\eta = \pi/12$ with $R = 6250$, $r = 0{\cdot}6$ has been tested against the results of Staniforth (1972). In Figures 4(a) and 4(b) time variations of the drag and lift coefficients, C_D and C_L are displayed, respectively, using three different grid types: a fine grid having $L \times P = 161 \times 161$, an intermediate grid with $L \times P = 121 \times 121$ and a coarse grid of $L \times P = 81 \times 81$ to demonstrate convergence of present computations. Figure 4(a) illustrates very good agreement with C_D and shows little dependence on the grid used while Figure 4(b) reveals that the computation of C_L does show some dependence on grid size. These diagrams also show Staniforth's results using both a numerical procedure and a series solution which is valid for small periods of time. The results of the present study agree well with those of Staniforth and the series solution for C_L departs from the numerical solution as time increases, as expected. It is noted that the cases and times considered in this study when $R = 10^3$, $\Omega = \pi$ and $r = 0{\cdot}5$ the computations are carried out using a finer grid in the z direction given by $L \times P = 201 \times 121$ to ensure that the outer boundary is placed far enough for larger values of time. Figures 5(a) and 5(b) show the calculated drag and lift coefficients for the case of $R = 10^3$, $\Omega = \pi$, $r = 0{\cdot}5 : \alpha = 0{\cdot}5$ and $\eta = \pi/4$ using three different outer boundary locations where $z_\infty = 8, 10, 12$. This numerical experimentation indicates

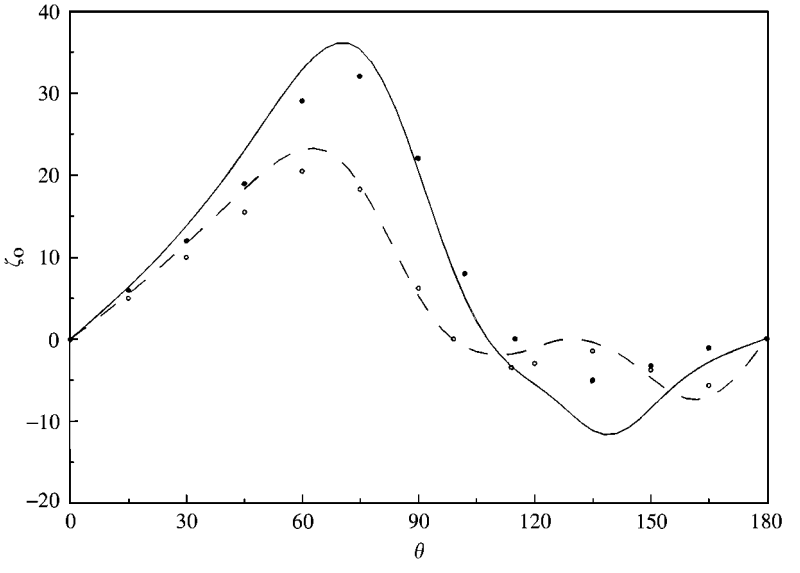

Figure 3. Comparison between the surface vorticity distribution obtained from the present study using the grid $L \times P = 121 \times 121$ and that obtained by Patel for the case of $R = 250$, $\Omega = 0$, $r = 0{\cdot}5878$, $\eta = \pi/2$ and $\alpha = 1{\cdot}0$. For $\tau = 1{\cdot}0$: ——, present; ●, Patel; for $\tau = 5{\cdot}0$: - - -, present; ○, Patel.

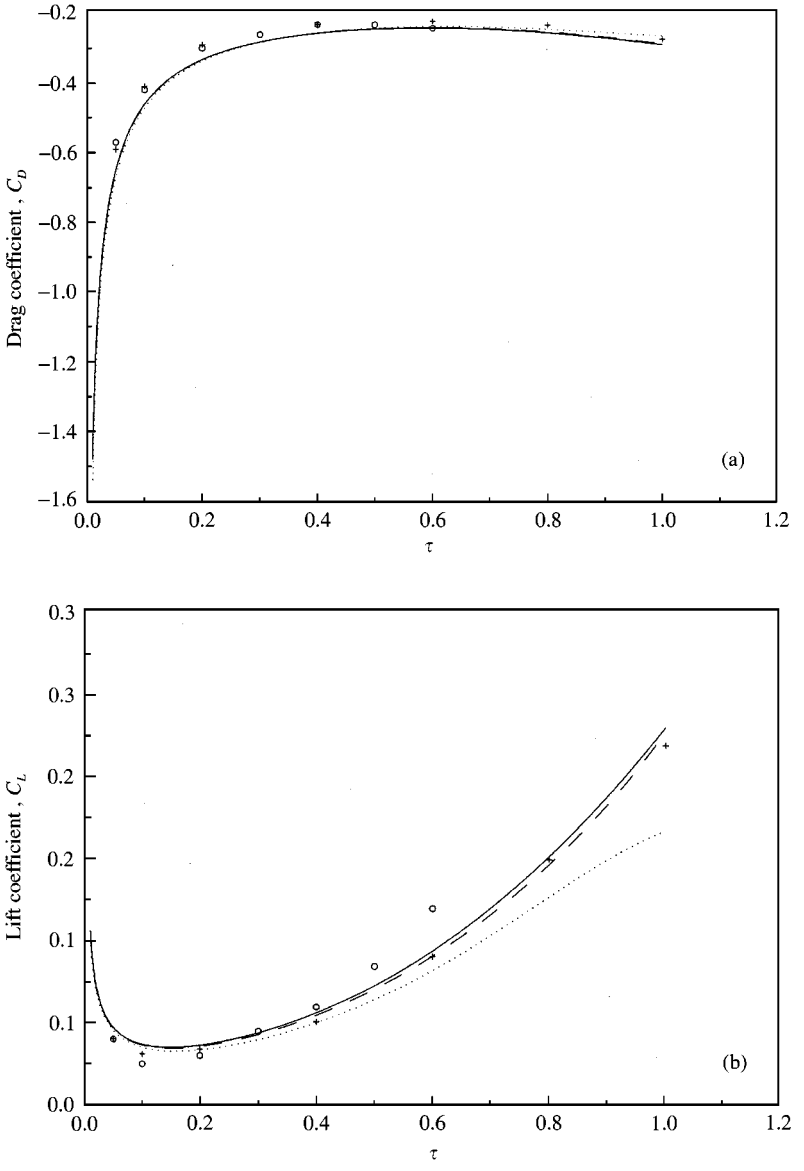

Figure 4. Variation of (a) drag coefficient and (b) lift coefficient with time for the case of $R = 6250$, $\Omega = 0$, $r = 0{\cdot}6$, $\eta = \pi/12$ and $\alpha = 1{\cdot}0$. The present study using grids: $L \times P = 161 \times 161$ (solid line), $L \times P = 81 \times 81$ (dotted line), $L \times P = 121 \times 121$ (dashed line). Staniforth's solution using: a numerical procedure (crosses) and a time-series solution (circles).

that there is essentially no change in going from $z_\infty = 10$ to 12; for the cases and times considered in this paper, $z_\infty = 12$ is a reliable outer boundary location for obtaining a highly accurate solution. Furthermore, this choice of z_∞ ensures that vorticity does not reach the outer boundary for the cases and times presented in this study. Thus, the application of the far-field boundary conditions (11) and (12) do not impose any unrealistic condition on the solution scheme. We point out that at $\tau = 0$ both C_D and C_L are infinite in magnitude due to the fact that the cylinder experiences infinite acceleration at that time and

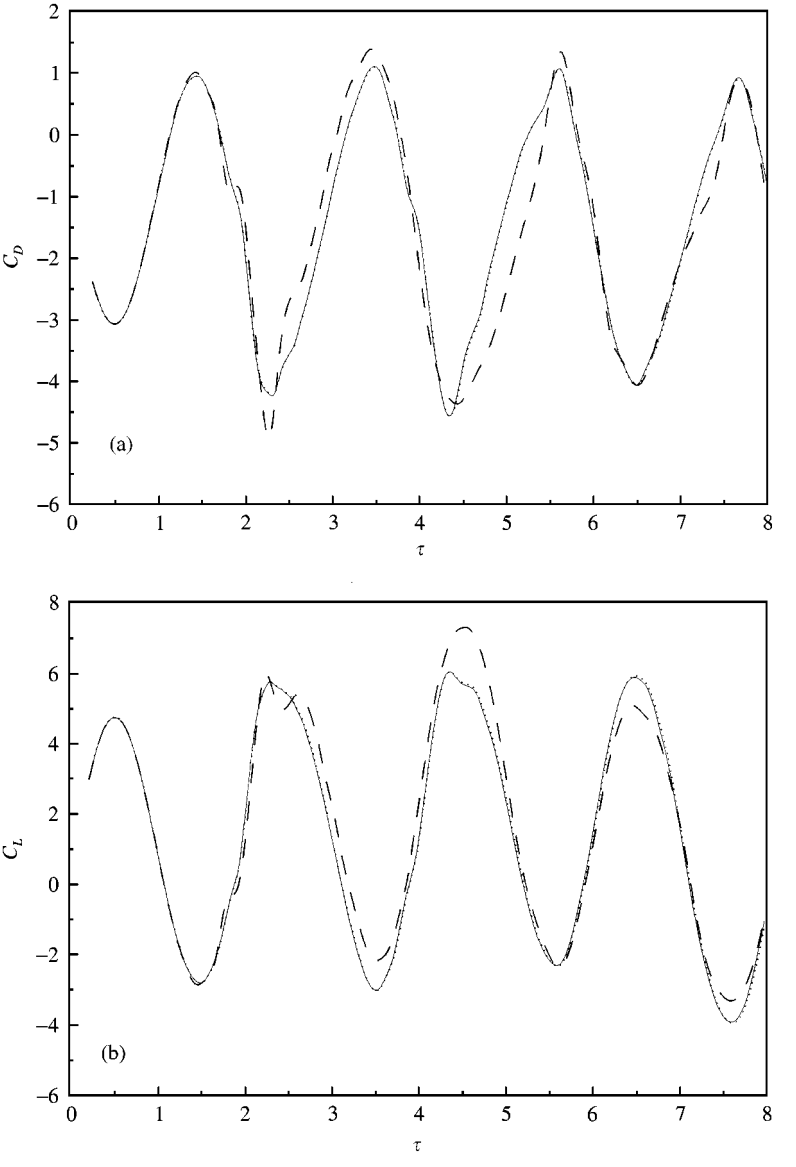

Figure 5. Variation of (a) drag coefficient and (b) lift coefficient with outer boundary location for the case of $R = 10^3$, $\Omega = \pi$, $r = 0{\cdot}5$, $\eta = \pi/4$ and $\alpha = 0{\cdot}5$: - - -, $z_\infty = 8$; …, $z_\infty = 10$; ——, $z_\infty = 12$.

then they both decrease rapidly. For this reason C_D and C_L are both plotted starting from $\tau = 0{\cdot}01$ in Figures 4 and 5.

The numerical results are grouped in two cases (i) $\eta = \pi/4$ and (ii) $\alpha = 0{\cdot}5$ with $R = 10^3$, $\Omega = \pi$ and $r = 0{\cdot}5$ to investigate effects of angle of inclination η and of the velocity ratio α, respectively. In the case of $\eta = \pi/4$ the problem is solved for two values of the velocity ratio, $\alpha = 0{\cdot}5$ and $1{\cdot}0$. On the other hand, the case of $\alpha = 0{\cdot}5$ is investigated for $\eta = \pi/4$ and $\pi/2$. The results are presented in the form of streamline patterns as well as the variations of the drag and lift coefficients with time. If L and D are the lift and drag on the cylinder, the total drag, C_D, and total lift, C_L, coefficients are defined by $C_D = D/\rho U^2 a$ and $C_L = L/\rho U^2 a$,

respectively. The drag and lift coefficients can be obtained from

$$C_D = \left[\frac{2\sinh\xi_0}{R}\int_0^{2\pi}\left(\frac{\partial\zeta}{\partial\xi}\right)_{\xi=0}\sin\theta\,\mathrm{d}\theta - \frac{2\cosh\xi_0}{R}\int_0^{2\pi}(\zeta)_{\xi=0}\sin\theta\,\mathrm{d}\theta\right]\cos\eta$$
$$+\left[\frac{2\cosh\xi_0}{R}\int_0^{2\pi}\left(\frac{\partial\zeta}{\partial\xi}\right)_{\xi=0}\cos\theta\,\mathrm{d}\theta - \frac{2\sinh\xi_0}{R}\int_0^{2\pi}(\zeta)_{\xi=0}\cos\theta\,\mathrm{d}\theta\right]\sin\eta, \quad (39)$$

$$C_L = \left[-\frac{2\cosh\xi_0}{R}\int_0^{2\pi}\left(\frac{\partial\zeta}{\partial\xi}\right)_{\xi=0}\cos\theta\,\mathrm{d}\theta + \frac{2\sinh\xi_0}{R}\int_0^{2\pi}(\zeta)_{\xi=0}\cos\theta\,\mathrm{d}\theta\right]\cos\eta$$
$$+\left[\frac{2\sinh\xi_0}{R}\int_0^{2\pi}\left(\frac{\partial\zeta}{\partial\xi}\right)_{\xi=0}\sin\theta\,\mathrm{d}\theta - \frac{2\cosh\xi_0}{R}\int_0^{2\pi}(\zeta)_{\xi=0}\sin\theta\,\mathrm{d}\theta\right]\sin\eta$$
$$-\pi\alpha\Omega(\sinh\xi_0)(\cosh\xi_0)\sin(\Omega\tau), \quad (40)$$

where the first and the third integrals in each gives the coefficient due to the pressure, C_{DP} and C_{LP} and the second and the fourth that due to friction, C_{DF} and C_{LF}. We note that the fifth term of C_L is the inviscid lift coefficient due to the accelerating imposed flow which would have been exerted on the fluid displaced by the cylinder [see Okajima *et al.* (1975) for the detailed derivation of the above formulas].

4.1. Streamline Patterns and Force Coefficients at $R = 10^3$, $\Omega = \pi$ and $r = 0.5$ when $\eta = \pi/4$

To discuss the effect of the velocity ratio on the vortex patterns and force coefficients, the flow is calculated with $\alpha = 0{\cdot}5$ and $1{\cdot}0$. Since all cases considered have $f = 0{\cdot}5$ or $T \equiv 1/f = 2$ as the period of cylinder oscillation, a complete cycle consists of the following four stages: at $\tau = 0$ the ellipse starts to oscillate with its maximum upward velocity and at $\tau = 0.5$ the ellipse reaches its maximum upward displacement and is in an instantaneous state of rest; at $\tau = 1$ the ellipse is in its equilibrium position and attains maximum velocity downward; at $\tau = 1{\cdot}5$ the ellipse is at its maximum downward displacement and is again in an instantaneous state of rest; and finally at $\tau = 2$ the ellipse is in its starting position and this pattern repeats itself.

Figure 6 shows 15 snap shots of the flow field for the case of $\alpha = 0{\cdot}5$ for the time interval $6 \le \tau \le 12$. This gives the details of the flow field structure during three complete cycles of oscillation following the first three cycles of oscillation. These plots, as seen in the moving reference frame of the cylinder, illustrate how the oncoming flow direction (from right to left) appears to periodically rotate. At even times it appears to approach the cylinder from above while at odd times it approaches the cylinder from below. At half times (i.e., $\tau = 6{\cdot}5$, $7{\cdot}5$, $10{\cdot}5$, $11{\cdot}5$) it appears to approach the cylinder horizontally since at these times the cylinder is momentarily at rest. During the first three cycles when $0 < \tau < 6$ (not shown here), the usual formations and detachments of upper (counterclockwise) and lower (clockwise) vortex pairs take place except at about $\tau = 4$. An interesting phenomenon occurs at $\tau = 4$: the two corotating vortex pairs are shed away to form adjacent vortices of the same sign coalescence. Figure 6(a–j) shows 10 snapshots of the flow covering the fourth complete cycle. During the interval $6 \le \tau \le 6{\cdot}5$ the counterclockwise vortex pair which was shed in the third cycle joins the counterclockwise vortex pair formed in the fourth cycle. With the increase of time these vortices become weak and move downstream [see Figure 6(f, g)] and fade away at $\tau = 7$ [Figure 6(h)]. In the time interval $7 \le \tau \le 11{\cdot}5$ no corotating adjacent vortex pairs appear but in the middle of the last quarter of the sixth cycle when $\tau = 11{\cdot}5$ [Figure 6(n)], we once again observe shedding of adjacent counterclockwise vortex pair

from the upper half of the cylinder. The vortices in the near wake are simply the result of one vortex shedding in each half cycle. This is the classical mode of single-vortex-shedding in each half-cycle leading to the formation of a Kármán street and the vortices in the near wake are shed at the rate of oscillation experienced by the cylinder.

For the higher velocity ratio $\alpha = 1{\cdot}0$, the computations are also carried out over six complete cycles. Figure 7(a–k) illustrates the flow for this case at 11 instants in time during the sixth cycle of oscillation. In this case, the flow appears to approach the cylinder along the major axis at even times, or along the minor axis at odd times, and horizontally at half times. Since the maximum oscillation speed is the same as the translational speed in this case, the oncoming flow appears to approach the cylinder at an angle of $\pi/4$ with the horizontal which exactly matches the inclination. Also, the streamlines are packed closer together here than in the case of $\alpha = 0{\cdot}5$. The explanation for this is that the speed of the oncoming flow is greater for $\alpha = 1{\cdot}0$ than it is for $\alpha = 0{\cdot}5$ and therefore results in streamlines spaced closer together. In the sixth cycle the near-wake structure is quite different from the ones obtained in the previous five cycles. During the interval $11{\cdot}35 \leq \tau \leq 11{\cdot}5$ we observe a double counter rotating vortex pair [see Figure 7(f)]. With the increase of time this double vortex pair splits up, and one of them joins with two upper vortex pairs to form a triple corotating vortex pair of the same sign coalescence at $\tau = 11{\cdot}55$ [Figure 7(h)]. Also, two corotating (clockwise) vortices join to form a double vortex pair in the very near-wake of the cylinder [Figure 7(g, h)]. Both double and triple corotating vortex pairs fade away at $\tau = 11{\cdot}6$.

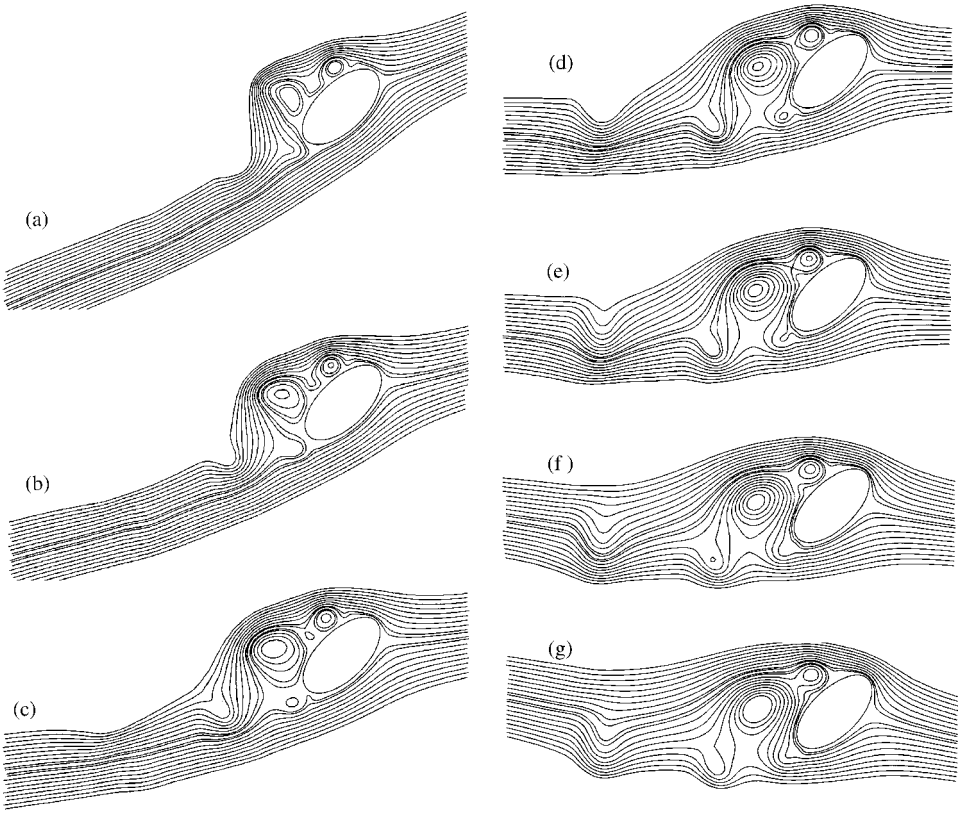

Figure 6. Instantaneous streamlines of the flow for $R = 10^3$, $\Omega = \pi$, $r = 0{\cdot}5$, $\eta = \pi/4$ and $\alpha = 0{\cdot}5$: (a) $\tau = 6$, (b) 6·25, (c) 6·35, (d) 6·45, (e) 6·5, (f) 6·55, (g) 6·6, (h) 7, (i) 7·5, (j) 8, (k) 10, (l) 10·5, (m) 11, (n) 11·5 and (o) 12.

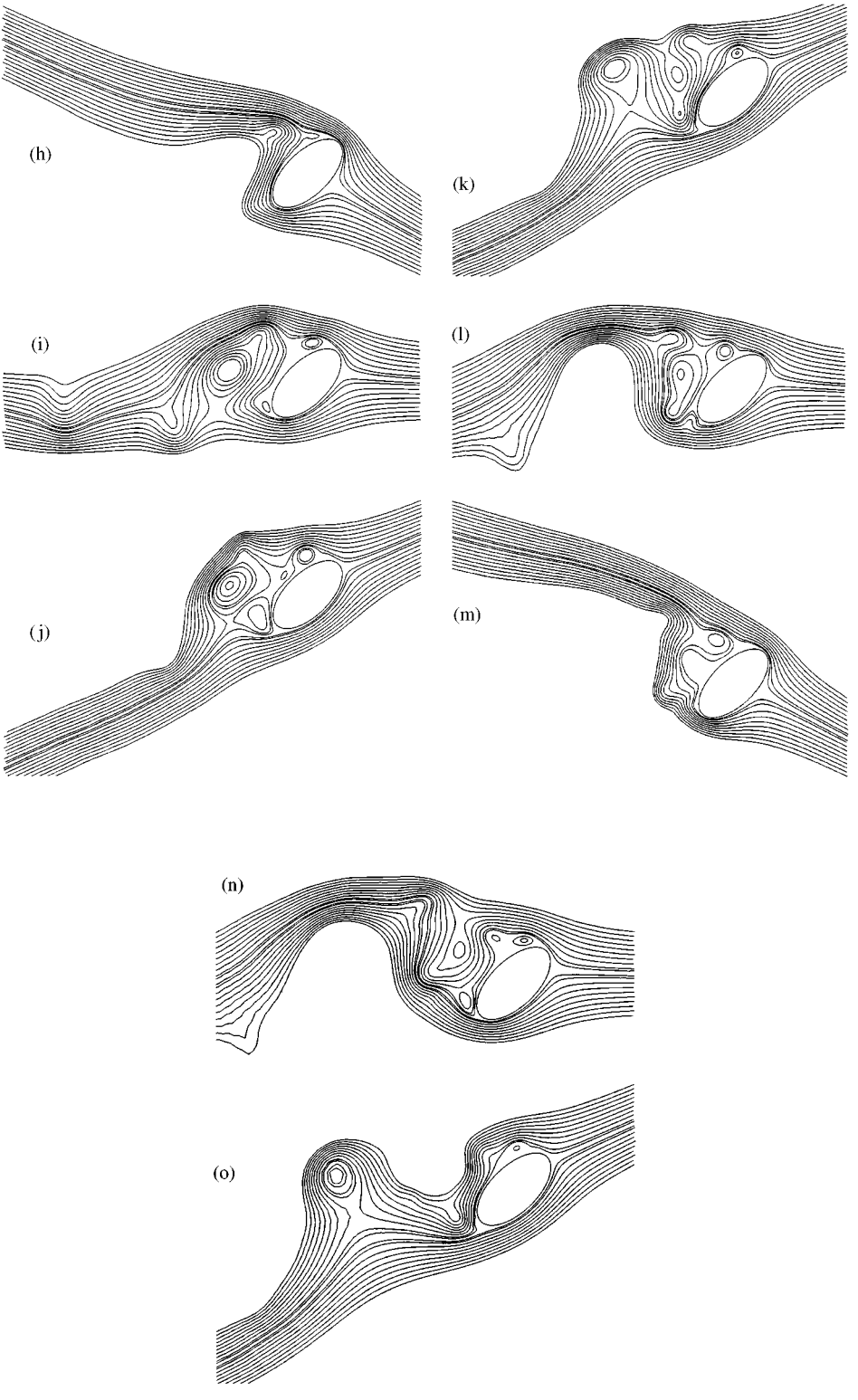

Figure 6. Continued.

It may be noted that this unusual feature in the wake, that is the presence of adjacent corotating vortices, was not reported in the elliptic cylinder cases previously but was reported in the accelerated circular cylinder case (Badr *et al.* 1996) and a periodic repetition of the phenomenon was recently reported by Dennis *et al.* (2000) in the rotationally oscillating and translating circular cylinder case. The fact that there is an unusual feature of this kind, production of double or triple corotating vortex pairs, in the near wake in an oscillating elliptic cylinder case is one of the essentially new contributions of our work. This kind of vortex pair interaction in the near-wake might be due to the oscillatory motion of the cylinder which tends to attract the two or three vortex pairs shedding away from the cylinder to each other, thus slowing down their convection further downstream. It is noted

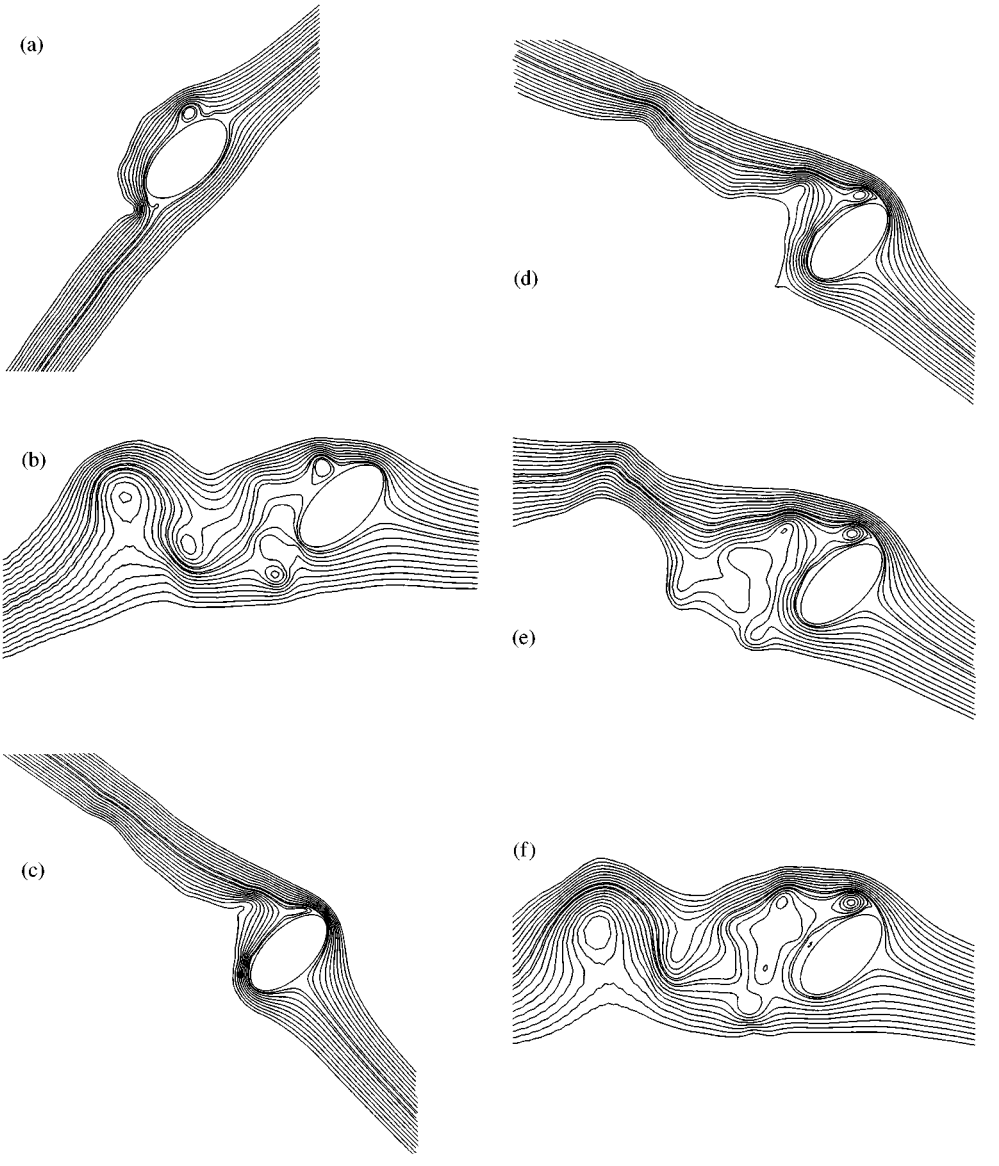

Figure 7. Instantaneous streamlines of the flow for $R = 10^3$, $\Omega = \pi$, $r = 0{\cdot}5$, $\eta = \pi/4$ and $\alpha = 1{\cdot}0$: (a) $\tau = 10$, (b) 10·5, (c) 11, (d) 11·25, (e) 11·35, (f) 11·45, (g) 11·5, (h) 11·55, (i) 11·6, (j) 11·75 and (k) 12.

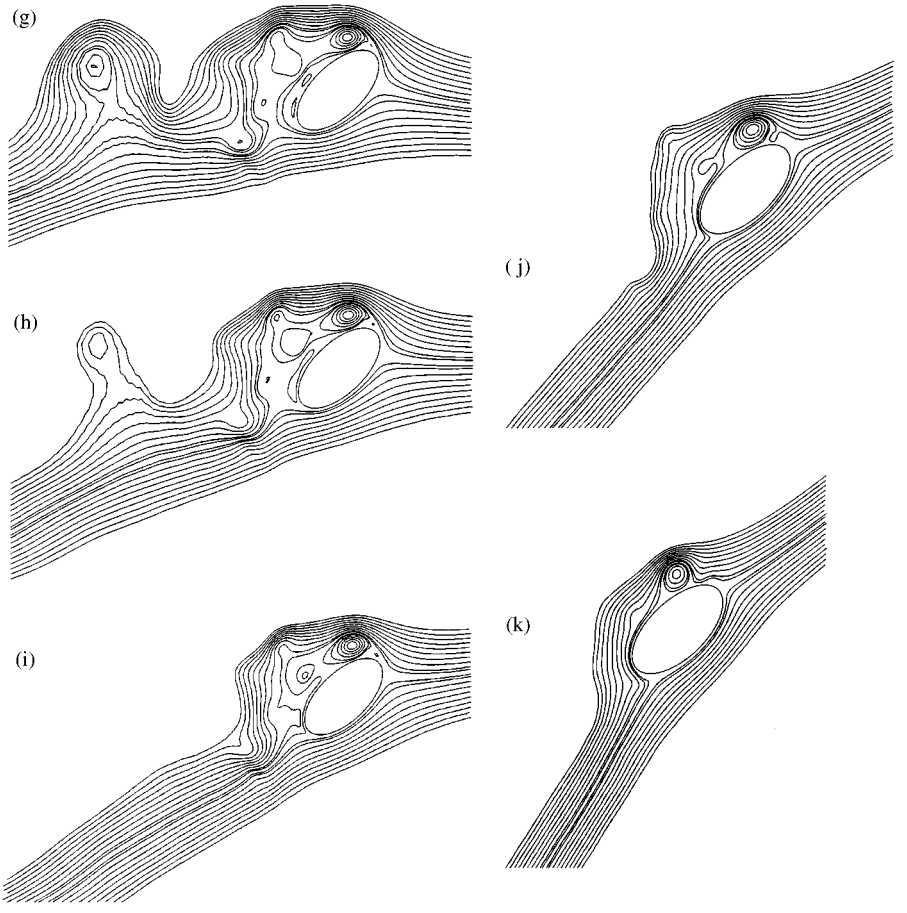

Figure 7. Continued.

that this unusual feature in the near-wake, the presence of two corotating vortices, was also reported in the experimental work by Öngören & Rockwell (1988, p. 215) in the cases of circular- and triangular-cross-section cylinders subject to controlled oscillations in a transverse direction to the incident flow.

Figures 8 and 9 show the variations of drag and lift coefficients when $\alpha = 0{\cdot}5$ and $1{\cdot}0$. These figures indicate the periodic variation of the flow field associated with vortex shedding. It appears that, the fluctuations in these coefficients are nearly periodic having a frequency equal to that of the forcing frequency of the cylinder and out of phase with each other. For both velocity ratios C_D and C_L reaches a maximum and a minimum value in the full cycle of the oscillation. It is noted that maximum values for C_L are attained near zero position of the cylinder during the upward and downward motion of the cylinder. The values of both C_D and C_L tend to be larger as the velocity ratio increases from $\alpha = 0{\cdot}5$ to $1{\cdot}0$ showing the effect of the oscillation on C_D and C_L when $\eta = \pi/4$.

4.2 Streamline Patterns and Force Coefficients at $R = 10^3$, $\Omega = \pi$ and $r = 0{\cdot}5$ when $\alpha = 0{\cdot}5$

To discuss the effect of the angle of inclination on the vortex patterns and force coefficients, the flow is calculated at $\eta = \pi/4$ and $\pi/2$. The results for the case of $\eta = \pi/4$ are presented in

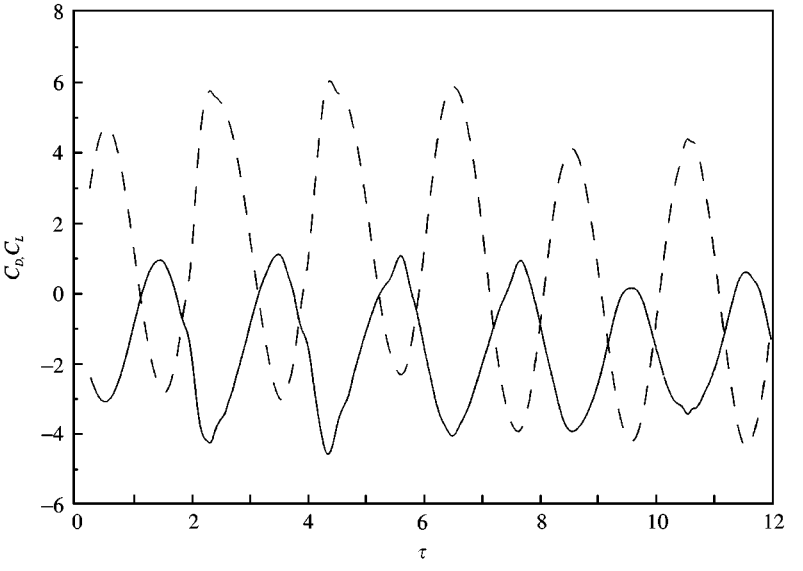

Figure 8. Variation of the total drag and lift coefficients, C_D and C_L, with τ at $R = 10^3$, $\Omega = \pi$, $r = 0{\cdot}5$, $\eta = \pi/4$ and $\alpha = 0{\cdot}5$: ——, C_D; ---, C_L.

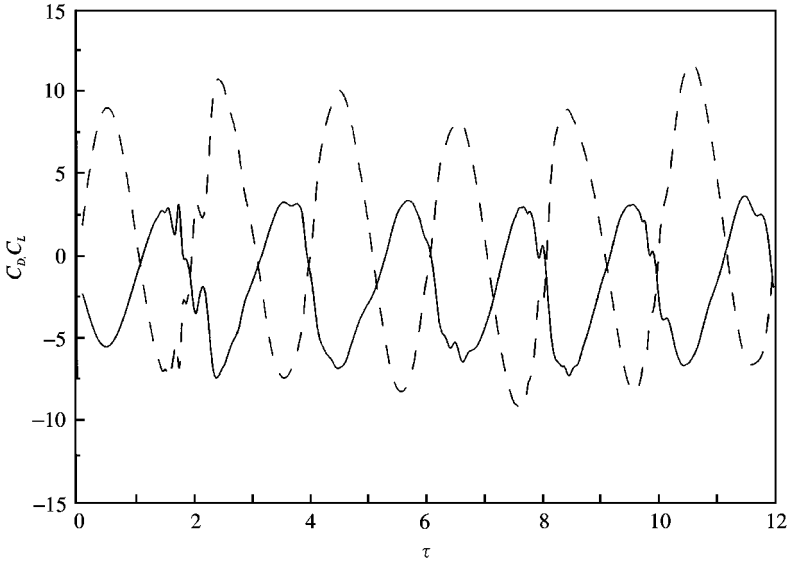

Figure 9. Variation of the total drag and lift coefficients, C_D and C_L, with τ at $R = 10^3$, $\Omega = \pi$, $r = 0{\cdot}5$, $\eta = \pi/4$ and $\alpha = 1.0$: ——, C_D; - - -, C_L.

Section 4.1(see Figures 6 and 8). The time variation of the streamline pattern for the case $\eta = \pi/2$ is shown in Figure 10(a–k) for selected values of τ between $\tau = 2$ and 16. Figure 10(a) shows the streamlines when the oscillatory velocity is zero. This figure shows a pair of symmetric vortices in the regions $90^\circ \leq \theta \leq 180^\circ$ and $180^0 \leq \theta \leq 270^\circ$. After a while, this vortex pair detaches and moves downstream, initiating the alternate shedding process. The interval between $\tau = 14$ and 16 represents the eighth complete oscillation cycle

following the start of the motion. Figure 10(g, i, k) represents the situation at the beginning, middle and end of the oscillation. On the other hand, Figure 10(h, j) represents the times at which the oscillatory motion comes to a complete rest. Figure 10 exhibits a single symmetrical mode of vortex formation: the streamline patterns show alternate, out-of-phase shedding of vortices from either side of the cylinder over an oscillation cycle; this is the classical mode of vortex shedding leading to formation of the Kármán street. The repetitive nature of the flow field in the near-wake can be observed from mirror image resemblances between the diagrams obtained in the last oscillation cycle for $\tau = 14$ and 15; $\tau = 14{\cdot}5$ and $15{\cdot}5$; $\tau = 15$ and 16 [see Figure 10(g–k)]. A check on the periodicity of the structure of the flow can be also performed by comparing the streamline patterns at times approximately one complete period apart: for example, the streamline patterns at $\tau = 14$ and 16 confirm almost exact periodic variations of the flow field in the near-wake as do streamline patterns at $\tau = 6$ and

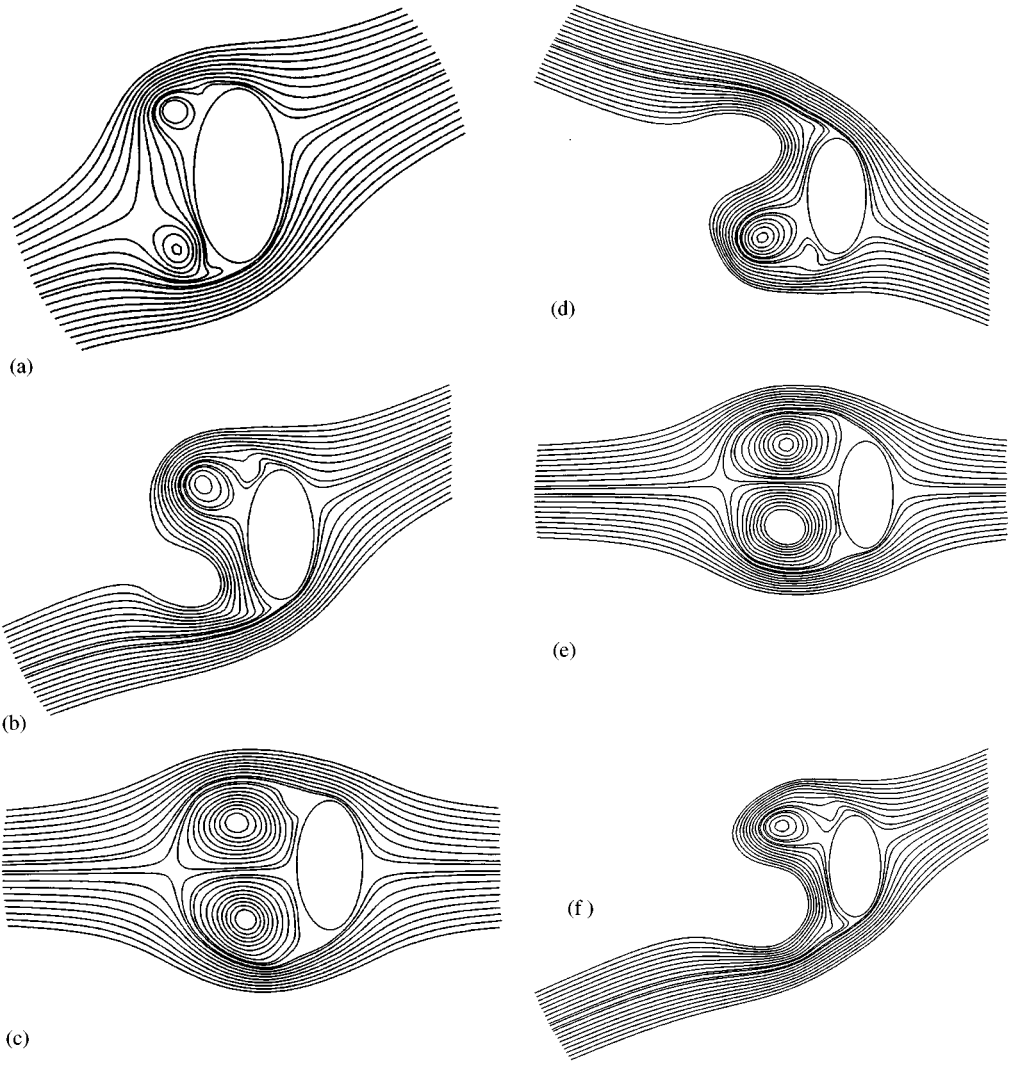

Figure 10. Instantaneous streamlines of the flow for $R = 10^3$, $\Omega = \pi$, $r = 0{\cdot}5$, $\alpha = 0{\cdot}5$ and $\eta = \pi/2$: (a) $\tau = 2$, (b) 4, (c) 4·5, (d) 5, (e) 5.5, (f) 6, (g) 14, (h) 14·5, (i) 15, (j) 15·5 and (k) 16.

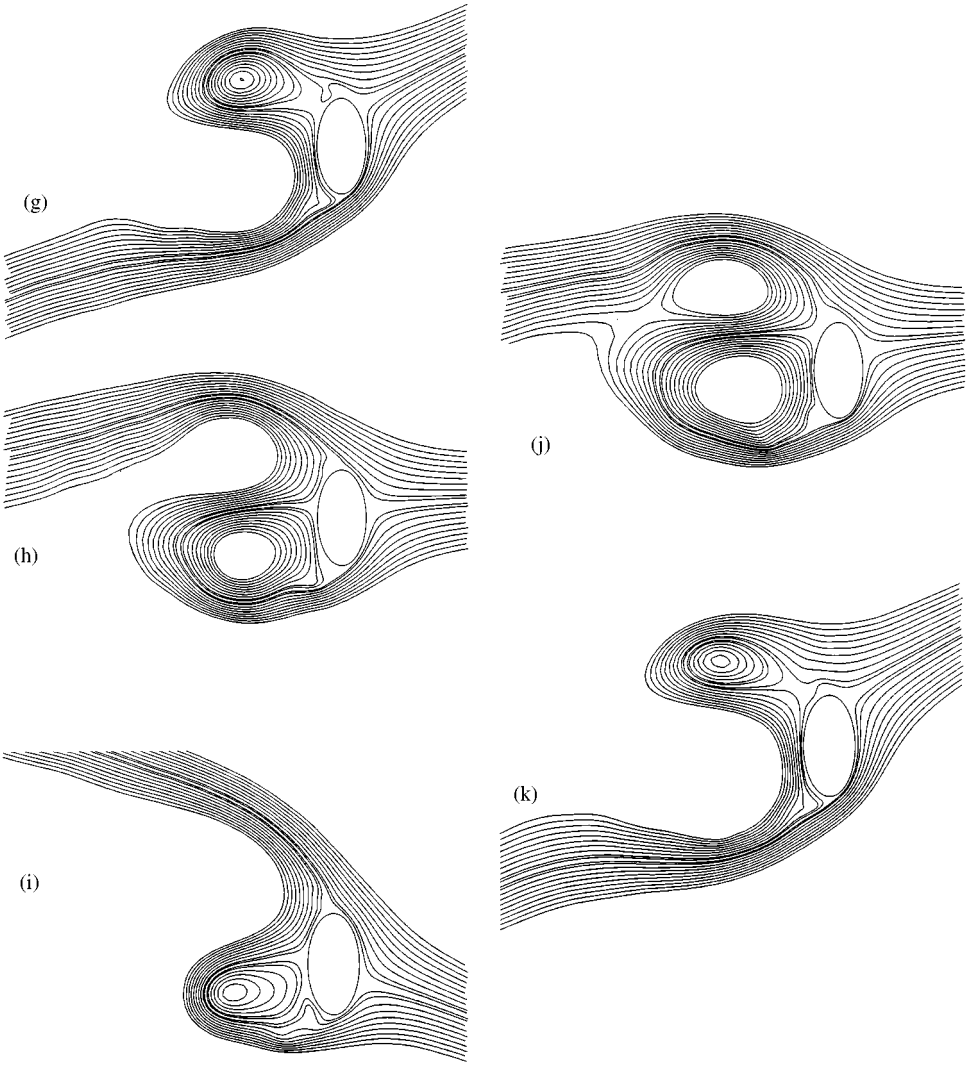

Figure 10. Continued.

8. Thus, the flow has almost settled down to a truly periodic state within only a few cycles of the oscillation.

Comparison of these figures with the corresponding ones in the case of $\eta = \pi/4$ indicates that although the vortices are the result of single vortex shedding in each half cycle of the oscillation, the near-wake structure is drastically different from the ones obtained in the case of $\eta = \pi/2$ and does not involve adjacent corotating coalescence in the case of $\eta = \pi/2$ unlike the case of $\eta = \pi/4$. The near-wake structure becomes much more organized and periodic as η increases from $\pi/4$ to $\pi/2$. Lastly, the vortex shedding process observed from the streamline patterns in Figure 10 for the case where $\eta = \pi/2$ is more predictable. Each oscillation of the ellipse appears to provoke vortex shedding from both tips with one being shed from the top during the first half of the cycle and another being shed from the bottom during the second half of the cycle. The vortices are probably shed at that part of the vibration cycle when the cylinder is near its maximum displacement.These counter-rotating

vortices grow to produce an almost symmetric pattern at times when the cylinder is momentarily at rest. During the next oscillation these shed vortices are then forced downstream as new ones are formed. Thus, an obvious effect of oscillation is to induce vortex shedding from the tips of the ellipse. This effect superposes itself on the usual vortex development around a purely translating elliptic cylinder. The ratio of the transverse to the longitudal spacing between vortices in the wake decreases slightly as the angle of inclination increases from $\pi/4$ to $\pi/2$ when $\alpha = 0{\cdot}5$. This is consistent with the experimental findings of Modi & Wiland (1970) in the case of stationary elliptic cylinder since the dominant velocity is the translational velocity when $\alpha = 0{\cdot}5$.

Figure 11 shows the time variation of the drag and lift coefficients. Here, the lift coefficient varies at the cylinder oscillation frequency, and drag coefficient oscillates at twice the cylinder oscillation frequency after a transition period when $\tau = 4{\cdot}0$ unlike the case of $\eta = \pi/4$ when $\alpha = 0{\cdot}5$. This feature, which is apparently a consequence of the geometry of the vortex street, is consistent with the experimental observations with no oscillation. It can be also seen that the increase of angle of inclination makes amplitude of the fluctuating lift force, C_L, smaller. In a recent numerical work of Badr *et al.* (2000) the two-dimensional unsteady viscous flow over an inclined elliptic cylinder placed in a uniform stream ($\Omega = 0$, $\alpha = 0$) is investigated numerically. Their calculated results for the case of $R = 10^3$, $r = 0{\cdot}6$ indicates that C_D curve shows nonperiodic behaviour in the case $\eta = 0$; whereas, in the case of $\eta = 30^\circ$, the C_D curve fluctuates at twice the vortex shedding frequency after the initial transition period. We note that for $\eta = \pi/2$ for a stationary cylinder $C_L = 0$ due to symmetry. For the oscillating case, during instants when the cylinder reaches its maximum upward and downward displacements the cylinder is temporarily at rest, and therefore the flow should be momentarily symmetric. This agrees with the computed flow observed in the streamline patterns of figure 10. The lift coefficient, C_L, is, however, not zero at these instants due to the inviscid lift imposed by the accelerating motion [see equation (40)]. The flow patterns and C_L are nearly periodic, and when averaged over a complete cycle $C_L = 0$. This is consistent with intuition. The above argument does not apply when $\eta = \pi/4$ since the flow is asymmetric and therefore much more complicated.

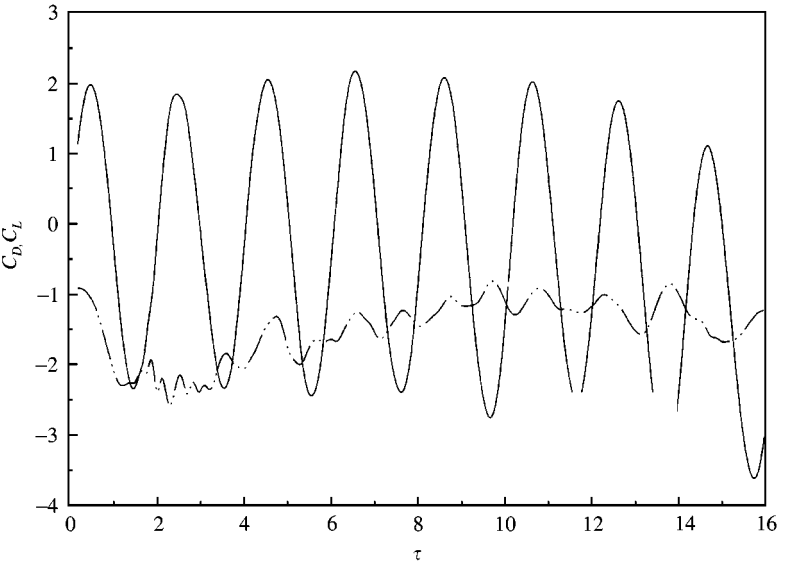

Figure 11. Variation of the total drag and lift coefficients: C_D and C_L with τ at $R = 10^3$, $\Omega = \pi$, $r = 0{\cdot}5$, $\alpha = 0{\cdot}5$ and $\eta = \pi/2$: ——, C_L; - · · -, C_D.

5. CONCLUSIONS

An implicit time-marching scheme was utilized to analyse the near-wake structure behind an inclined elliptic cylinder as well as the fluid forces acting on a cylinder, where the cylinder was subject to rectilinear oscillations in a transverse direction to the oncoming flow. The numerical scheme was tested by modifying it to solve the special case of pure translation. The effects of the velocity ratio and the angle of inclination are discussed. In the case of $\eta = \pi/4$ the results are obtained in a range of velocity ratio $0{\cdot}5 \leq \alpha \leq 1{\cdot}0$ at the Reynolds number of $R = 10^3$ and the forcing Strouhal number $\Omega = \pi$ when $\alpha = 1{\cdot}0$. An interesting phenomenon occurs in the case of $\eta = \pi/4$ when $\alpha = 0{\cdot}5$ and $1{\cdot}0$. In the case of $\alpha = 0{\cdot}5$ the two corotating vortex pairs are shed away from the cylinder to form two adjacent corotating vortices in the near-wake region whereas in the case of $r = 0{\cdot}5$ both double and triple corotating vortex pairs occur in the cylinder wake. This seems to delay the development of the periodic flow pattern in the near-wake. Force coefficients show periodic behaviour when $\alpha = 0{\cdot}5$ and $1{\cdot}0$ with a frequency equal to that of the forcing frequency of the cylinder and they are out of phase with each other.

In the case of $\alpha = 0{\cdot}5$ the results are obtained at two values of angle of inclination $\eta = \pi/4$ and $\pi/2$ in the case of the Reynolds number of $R = 10^3$ and the forcing Strouhal number $\Omega = \pi$ when $r = 0{\cdot}5$. It is found that for the cases of $\pi/2$ the near-wake does not involve adjacent corotating vortices.

In all cases considered in this study C_L curve oscillates with the forcing frequency of the cylinder whereas a switch over in the nature of the fluctuations of the drag coefficient is observed with the increase of angle of inclination.

In summary, therefore, we have observed some new fluid mechanical phenomena in this type of flow, particularly with regard to the facts about the production of the double or triple corotating vortex shedding for certain values of η and α and the behaviour of the drag coefficient as η increases.

ACKNOWLEDGEMENTS

The support of the Natural Sciences and Engineering Research Council of Canada is gratefully acknowledged.

REFERENCES

BADR, H. M. 1994 Oscillating viscous flow over an inclined elliptic cylinder. *Ocean Engineering* **21,** 401–426.

BADR, H. M. DENNIS, S. C. R. & KOCABIYIK, S. 1996 Symmetrical flow past an accelerated circular cylinder. *Journal of Fluid Mechanics* **308,** 97–110.

BADR, H. M. DENNIS, S. C. R. & KOCABIYIK, S. Numerical simulation of the unsteady flow over an elliptic cylinder at different orientations. *International Journal for Numerical methods in Fluids* (in press).

BADR, H. M. & KOCABIYIK, S. 1997 Symmetrically oscillating viscous flow over an elliptic cylinder. *Journal of Fluids and Structures* **11,** 745–766.

BLACKBURN, H. M. & HENDERSON, R. D. 1999 A study of two-dimensional flow past an oscillating cylinder. *Journal of Fluid Mechanics* **385,** 255–286.

DAVIDSON, B. J. & RILEY, N. 1972 Jets induced by oscillatory motion. *Journal of Fluid Mechanics* **53,** 287–303.

D'ALESSIO, S. J. D., DENNIS, S. C. R. & NGUYEN, P. 1999 Unsteady viscous flow past an impulsively started oscillating and translating elliptic cylinder. *Journal of Engineering Mathematics* **35,** 339–357.

DENNIS, S. C. R. & GAU-ZU CHANG, 1969 Numerical integration of the Navier–Stokes equations in two-dimensions. Mathematics Research Center, University of Wisconsin, Technical Summary Report No. 859.

DENNIS, S. C. R. & KOCABIYIK, S. 1991 An asymptotic matching condition for unsteady boundary-layer flows governed by the Navier–Stokes equations. *IMA Journal of Applied Mathematics* **47,** 81–98.

DENNIS, S. C. R., NGUYEN, P. & KOCABIYIK, S. 2000 The flow induced by a rotationally oscillating and translating circular cylinder. *Journal Fluid Mechanics* **407,** 123–143.

DENNIS, S. C. R. & QUARTAPELLE, L. 1989 Some uses of Green's Theorem in solving the Navier–Stokes equations. *International Journal of Numerical Methods in Fluids* **9,** 871–890.

GRAHAM, J. M. R. 1993 Comparing computation of flow past circular cylinders with experimental data. In *Bluff Body Wakes, Dynamics and Instabilities*, pp. 317–324. New York: Springer.

GRIFFIN, O. M. & RAMBERG, S. E. 1974 The vortex-street wakes of vibrating cylinders. *Journal of Fluid Mechanics* **66,** 553–576.

HALL, P. 1984 On the stability of the unsteady boundary layer on a cylinder oscillating transversely in a viscous fluid. *Journal of Fluid Mechanics* **146,** 347–367.

MODI, V. J. & WILAND, E. 1970 Unsteady aerodynamics of stationary cylinders. *AIAA Journal* **8,** 1814–1821.

NAIR, M. T. & SENGUPTA, T. K. 1997 Unsteady flow past elliptic cylinders. *Journal of Fluids and Structures* **11,** 555–595.

NOVAK, M. & TANAKA, H. 1977 Pressure correlations on a vibrating cylinder. In *Proceedings of the 4th International Conference on Wind Effects on Buildings and Structures*, Heathrow, London, 1975 (ed. K. J. Eaton), pp. 227–232. Cambridge, U.K.: Cambridge University Press.

OKAJIMA, A., TAKATA, H. & ASANUMA, T. 1975 Viscous flow around a transversally oscillating elliptic cylinder. *Institute of Space and Aeronautical Science*, University of Tokyo, Report No. 533.

ÖNGÖREN, A. & ROCKWELL, D. 1988 Flow structure from an oscillating cylinder Part 1. Mechanism of phase shift and recovery in the near wake *Journal of Fluid Mechanics* **191,** 197–223.

PATEL, V. A. 1981 Flow around the impulsively started elliptic cylinder at various angles of attack. *Computers and Fluids* **9,** 435–462.

RAMBERG, S. E. & GRIFFIN, O. M. 1976 Velocity correlation and vortex spacing in the wake of a vibrating cable. *ASME Journal of Fluids Engineering* **98,** 10–18.

SZEPESSY, S. & BEARMAN, P. W. 1992 Aspect ratio and end plate effects on vortex shedding from a circular cylinder. *Journal of Fluid Mechanics* **234,** 191–218.

STANIFORTH, A. N. 1972 Studies of symmetrical and asymmetrical viscous flows past impulsively started cylinders. Ph.D. Thesis, University of Western Ontario, London, Ontario, Canada.

TANEDA, S. 1977 Visual study of unsteady separated flows around bodies. *Progress in Aerospace Sciences* **17,** 287–348.

TOEBES, G. H. 1969 The unsteady flow and wake near an oscillating cylinder. *ASME Journal of Basic Engineering* **91,** 493–502

WILLIAMSON, C. H. K. 1988 The existence of two stages in the transition to three-dimensionality of a circular wake. *Physics of Fluids* **31,** 3165–3168.

WILLIAMSON, C. H. K. & ROSHKO, A. 1988 Vortex formation in the wake of an oscillating cylinder. *Journal of Fluids and Structures* **2,** 355–381.